
Geometric feature performance under downsampling for EEG classification tasks

Bryan Bischof
Stitch Fix Algorithms
Berkeley, CA
bryan.bischof@gmail.com

Eric Bunch
American Family Insurance
Madison, WI
eric.a.bunch@gmail.com

Abstract

We experimentally investigate a collection of feature engineering pipelines for use with a CNN for classifying eyes-open or eyes-closed from electroencephalogram (EEG) time-series from the Bonn dataset. Using the Takens’ embedding—a geometric representation of time-series—we construct simplicial complexes from EEG data. We then compare ϵ -series of Betti-numbers and ϵ -series of graph spectra (a novel construction)—two topological invariants of the latent geometry from these complexes—to raw time series of the EEG to fill in a gap in the literature for benchmarking. These methods, inspired by Topological Data Analysis, are used for feature engineering to capture local geometry of the time-series. Additionally, we test these feature pipelines’ robustness to downsampling and data reduction. This paper seeks to establish clearer expectations for both time-series classification via geometric features, and how CNNs for time-series respond to data of degraded resolution.

Introduction

Topological Data Analysis (TDA) (Zomorodian and Carlsson [2004], Edelsbrunner et al. [2000]) has gained much attention due to applications for data analysis and machine learning. In particular, persistent homology (Scopigno et al. [2004], Edelsbrunner et al. [2002]) has been leveraged for machine learning purposes in numerous tasks. The methods attempt to describe the shape of the data in a latent space particularly amenable to feature engineering. The efficacy of topological features has been demonstrated in various tasks (Chazal and Michel [2017], Dindin et al. [2020]).

In this paper, we investigate the performance of various topological feature engineering approaches for EEG time-series classification using one dimensional CNN as the classifiers. While CNN architectures are heavily experimented on, less research has explored models for feature engineering using modern geometric techniques (Seo et al. [2016], Bronstein et al. [2017]). Usually, CNNs are trained on the raw time-series data where a convolutional kernels of a fixed sizes and strides are applied to the series with moving windows to compute higher-order features. Persistent homology of the *Takens’ embedding* provides one geometric procedure to engineer features for a time-series (Umeda [2017]).

For a time-series, the k -dimensional *Takens’ embedding* of the time-series is the Euclidean embedding of points defined by a sliding window of size k —this provides a point-cloud representation of the time-series. From this point cloud the common TDA approach to compute homology of the ϵ -Rips complex provides persistent features. Both the raw series and the persistent features can be exploited for machine learning tasks. As a first step towards better understanding of feature engineering on time-series, we compare the performance of these two approaches for the classification task.

Furthermore, we propose a novel geometric method beyond homology theories utilizing eigenvalues of sequences of graph Laplacians. Again, we utilize the point-cloud representation’s ϵ -neighbor graph,

and compute the normalized graph Laplacians' eigenvalues. Density counts of these eigenvalues are encoded as m discrete ϵ -series. We demonstrate the superiority of our approach over the homological features and compare to the raw time-series via classification experiments while keeping the classifier architecture fixed.

Generally, neural networks are optimized via network features like batch size, learning rate, kernels, pooling layers, and the like. Some papers have experimented with data resizing to improve training time — in (Howard [2018]) they introduced dynamic resizing with progressive resolution; (Roy et al. [2018]) have investigated the CNN robustness under noise. We have not found in the literature examinations of explicit downsampling algorithms' effects. To this effect, we study the performance of the feature engineering methods across multiple regimes. We vary features, time-series resolution, effective resolutions, and compare degradation across the feature types and downsampling methods—a practice common in the signal processing literature but less so in classification of time-series. Note that the encoding methods in this paper need not only apply to sequential collections.

The principal contributions of this work include:

- Introduce a new feature engineering technique utilizing latent geometric properties of the time series.
- Apply the theory and methods of downsampling to time-series classification problem.
- Propose and demonstrate a comparison framework and baseline results for time series clustering via varying features and CNN architectures.

Comments and Caveats

In machine learning tasks, especially those with more complicated models, it is essential to attempt to establish a baseline, a set of target metrics, and a comparison pipeline for apples-to-apples evaluation—in some literature this is called boat-racing, or horse-racing. During our literature review of TDA methods for the EEG prediction dataset, we did not find sufficient comparators and thus integrate this into our experimentation goals, whence the large volume of experiments considered in this paper.

We do not treat the neuroscience topics necessary for a deeper investigation of EEG technology or seizures. We treat the dataset as a mathematical task, and focus instead on the models and methods in machine learning. In particular, as highlighted in (Covert et al. [2019]) EEG datasets are structural time series, i.e. physical geometry of data collection correlates with relationships between series. We use only local readings thus reducing this covariance structure. Furthermore, train and test splitting can be challenging as several samples are taken from the same patient. For these, and other reasons, we make no comparison to SOTA networks. **The methods and architectures covered in this work are not state-of-the-art in terms of performance.**

This work in context

Generally, CNN architectures are optimized via network features like batch size, learning rate, kernels, pooling layers, and the like. Some papers have experimented with resizing to improve training time — in (Howard [2018]) they introduced dynamic resizing with progressive resolution. Others (Roy et al. [2018]) have investigated the robustness of CNN performance under image degradation due to noise, but we've not found in the literature examinations of explicit downsampling algorithms' effects. There is renewed interest in small models over the last few years in other ML tasks; for time-series prediction this paper provides one such framework for pursuing those ends.

For a collection classification task, the encoding of the data itself is also at opportunity for tuning. While common approaches to sequential data sets use RNNs and LSTMs to take advantage of data characteristics like autoregressive features, the encoding methods in this paper need not only apply to sequential collections.

We wish to highlight that while time series classification is well studied and has clear and effective baselines (Wang et al. [2017]), EEG classifiers are of great value and remain elusive.

1 Methods

We use two geometric methods for feature engineering, persistent Betti numbers and persistent Spectra. The first is a development of Umeda [2017], the second is a new construction.

Takens' Embedding Given a time series, $\{t_i\}_{i=0}^n \subset \mathbb{R}$, and a function $f : \mathbb{R} \rightarrow \mathbb{R}$. Then the *Takens' embedding* with window size m , denoted T^m , is the collection of points in \mathbb{R}^m given by

$$\{[f(t_0), f(t_1), \dots, f(t_{m-1})], [f(t_1), f(t_2), \dots, f(t_m)], \dots, [f(t_{n-m+1}), f(t_{n-m+1}), \dots, f(t_n)]\}$$

That is, T^m is the collection of points in \mathbb{R}^m given by taking sliding windows over the time series $f(t_i)$. For volatile series, smooth transformations on this geometry are known to preserve properties of the time series, such as the dimension of chaotic attractor, and Lyapunov exponents of the dynamics.

ϵ -neighbor graph Given a finite subset $X \subset \mathbb{R}^m$ with n points, and a real number $\epsilon \geq 0$ we form the ϵ -graph $G_\epsilon(X)$ with nodes of $G_\epsilon(X)$ indexed by the elements of X , and edges $v_x \rightarrow v_y$ for $x, y \in X$ if and only if $\|x - y\| < \epsilon$.

Persistent Homology and Time Series Analysis In (Umeda [2017]), the author calculates persistent Betti numbers(c.f. the appendix: A for definitions) of EEG time series signals via the aforementioned Persistent Betti-number model pipeline before feeding the output into a CNN for an eyes open/closed prediction task. In particular, for time series $\{f(t_i)\}_{i=0}^n$, consider T^m its Takens' embedding as the enumerated subset in \mathbb{R}^m , then compute $\beta_k(\epsilon)$ for all $0 \leq k < m$ and $\epsilon \in [0, r]$.

Graph Laplacians Spectral graph theory is an integral facet of graph theory (Chung and Graham [1997]) and one of the key objects of this theory is the Laplacian matrix of a graph, as well as its eigenvalues. We assume all graphs are undirected and simple. For a graph G , let A and D be the adjacency matrix and the degree matrix of G respectively.

The *Laplacian* of G is defined to be $L = D - A$. The *normalized Laplacian* of G is then defined to be $\tilde{L} = D^{-1/2}AD^{-1/2}$.

Denote the eigenvalues(or *spectrum*) of \tilde{L} by $0 = \lambda_0 \leq \lambda_1 \leq \dots \leq \lambda_{n-1}$. You may recall:

[Lemma 1.7, Chung and Graham [1997]] For a graph G with n vertices, we have that

1. $0 \leq \lambda_i \leq 2$, with $\lambda_0 = 0$.
2. If G is connected, then $\lambda_1 > 0$. If $\lambda_i = 0$ and $\lambda_{i+1} \neq 0$ then G has exactly $i + 1$ connected components.

Persistent Laplacian Eigenvalues for Time Series Analysis Denote by $\tilde{L}_\epsilon(X)$ the normalized Laplacian of $G_\epsilon(X)$. Define $\hat{\lambda}_\epsilon(X) = [\lambda_\epsilon(X)_0, \lambda_\epsilon(X)_1, \dots, \lambda_\epsilon(X)_{n-1}]$ to be the vector of eigenvalues of $\tilde{L}_\epsilon(X)$, in ascending order: $0 = \lambda_\epsilon(X)_0 \leq \lambda_\epsilon(X)_1 \leq \dots \leq \lambda_\epsilon(X)_{n-1} \leq 2$. When the context is understood, we will drop the designation (X) in the above notations; e.g. G_ϵ or $\lambda_{\epsilon 0}$.

Let I be an interval, $\hat{v} = [v_0, v_1, \dots, v_{n-1}]$ be a vector, and define

$$\mathbf{count}_I(v) := \#\{v_i \mid v_i \in I\}. \quad (1)$$

For a given interval $[0, r]$ (this will be our range of resolutions), and a finite collection of real numbers $0 = \tau_0 < \tau_1 < \dots < \tau_k = 2 + \delta$ for any fixed δ , such that $0 < \delta \in \mathbb{R}$. For $\epsilon \in [0, r]$, define:

$$\mu_j(\epsilon) := \mathbf{count}_{[\tau_j, \tau_{j+1})}(\hat{\lambda}_\epsilon) \text{ for } 0 \leq j \leq k - 1 \quad (2)$$

That is, $\mu_j(\epsilon)$ counts the number of eigenvalues of \tilde{L}_ϵ that lie between τ_j and τ_{j+1} . Observe that $\mathbf{count}_{[0,0]}(\hat{\lambda}_\epsilon)$ is equal to the number of connected components of G_ϵ . We will view the collection $\{\mu_j\}$ as a collection of j real-valued functions with domain $[0, r]$. We refer to the collection of μ_j 's as *persistent Laplacian eigenvalues*. Given a time series $\{f(t_i)\}_{i=0}^n$ we form T^m , and compute $\{\mu_j\}_{j=0}^l$ for some choice of τ_0, \dots, τ_l .

Overview of model pipelines

Raw Time Series Features: We feed the sequential time-series values into our CNN architecture.

Persistent Betti Numbers Features: We encode each time series with the ‘k-step’ Takens’ embedding into \mathbb{R}^k . This point cloud’s ϵ -neighbor graph generates the Vietoris-Rips filtration up to dimension 3. The order of the degree n simplicial homology (or n ’th Betti number) is computed for each ϵ neighbor complex, and encoded as n discrete ϵ -series. We feed the sequential ϵ -series values — each on their own channel — into our CNN architecture.

Persistent Laplacian Eigenvalue Features: We encode each time series with the ‘k-step’ Takens’ embedding into \mathbb{R}^k . This point cloud’s ϵ -neighbor graph is collected and it’s normalized graph Laplacians are computed. The eigenvalues of these Laplacians are computed and bucketed into a partition of m buckets. The counts of eigenvalues in each bucket are encoded as m discrete ϵ -series. We feed the sequential ϵ -series values — each on their own channel — into our CNN architecture.

Experimental design: In each of the pipelines, we prepend the model pipeline with a downsampling step using one of three downsampling algorithms and several downsampling resolutions (c.f. the appendix B). Our design matrix consists of the three downsampling methods applied to $\{200, 300, 400, 500, 600\}$ initial data lengths downsampled by multiples of 50. Each of these initial data sets are fed through each of the model pipelines and subsequent CNNs. We use cross-validation and accuracy to evaluate the performance.

2 Experiments

Data set and classification task The data used in this work are time series EEG signals, and are provided by the University of Bonn, explored in Andrzejak et al. [2001]. This data set is comprised of five sets (labeled A-E), each containing 100 single-channel EEG segments 23.6 seconds in duration, with 4097 observations. The segments were hand selected from within a continuous single-channel EEG recording, chosen for absence of artifacts as well as fulfilling a stationarity condition. Set E contains segments of seizure activity, sets C and D are taken from epilepsy patients during an interval where no seizure activity was occurring, and sets A and B are observations from non epilepsy diagnosed patients. The observations in set A occur during times when the patient’s eyes were open, while those in set B occur during times when the patient’s eyes were closed. We study the classification task of A vs. B., i.e. eyes open or closed.

CNN architectures All of the prediction algorithms used in this paper are CNNs, each with two sets of one dimensional convolution and max pool layers, followed by a fully connected layer to predict the class label. Architecture parameters are vectors representing $\langle \text{input, channels, factor, kernel1 size, kernel2 size} \rangle$; $\langle \text{res, 1, 5, (res/600) * 18, 2} \rangle$, $\langle 300, 3, 7, 6, 2 \rangle$, $\langle 300, 7, 3, 6, 2 \rangle$ for raw time-series, Betti numbers, and eigenvalues respectively. factor refers to the multiplicative factor of input channels to output channels in each convolution layer, and res refers to the resolution to which the time series

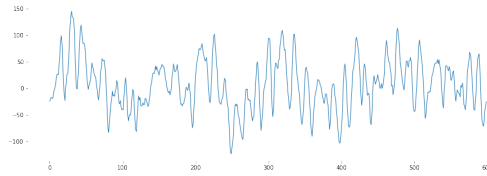


Figure 1: Raw time series from a segment of time where the patient’s eyes were closed, a segment of 600 time steps, not downsampled. The x-axis is in units of time-steps and the y-axis is μV amplitude

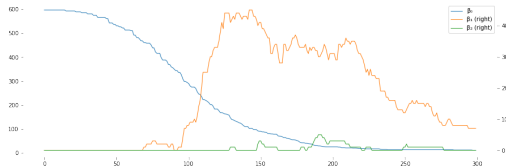


Figure 2: $\beta_j(\epsilon)$ computed for the time series shown in Fig. 1. The x-axis is in units of ϵ -steps and the y-axis is the counts identified by legend.

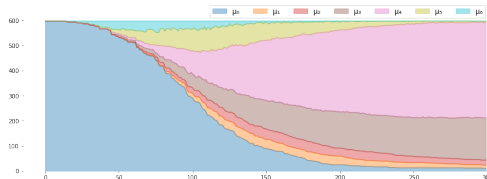


Figure 3: Area plot of $\mu_j(\epsilon)$, i.e. percentage of binned eigenvalues, for the time series in Fig. 1. The x-axis is in units of ϵ -steps and the y-axis is the counts.

was downsampled to. Stride and dilation in both conv layers are 1 for each model; first pooling layer has size 7, second has size 3; each model is trained for 10 epochs. Longer training was explored but in testing, more than ten epochs showed little improvement in performance.

Experiments and Results For a given observation length, downsampling method, and downsampling rate, we run 10-fold cross validation for each of the three prediction methods described. The average and standard deviation of accuracy is recorded and displayed in Figure 4 for non-dynamic bucketing downsampling methods, and Figure 5 for dynamic bucketing downsampling methods.

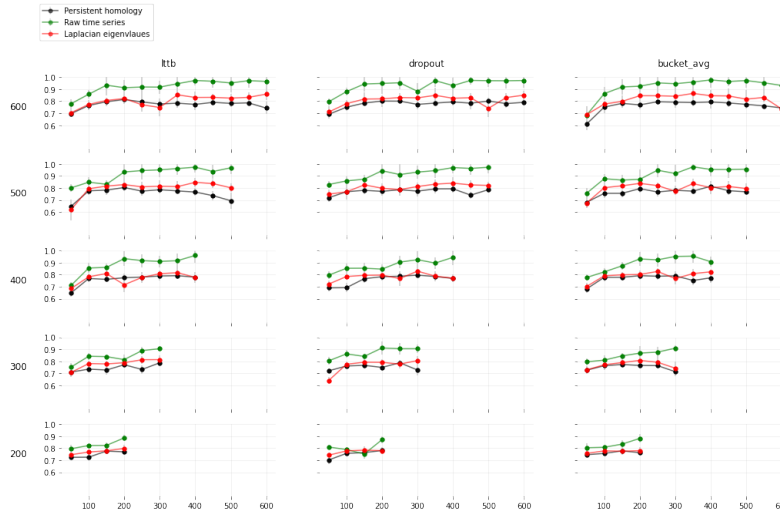


Figure 4: Experiment results for non dynamic bucketing downsampling methods. Diagram rows correspond to initial length of time-series segment, with each point reflecting number of points after downsampling. Within rows, y-axis is accuracy on binary cross-entropy, x-axis is the number of points in the time-series samples.

3 Outcomes

We’ve explored a collection of ‘experiments’ in training and testing CNNs built on EEG data to predict if a patient’s eyes are open or closed. The aforementioned experiments primarily sought to establish performance comparisons while varying the feature engineering choice, the chunk size, and the downsampling resolution used.

We established a baseline performance using a raw time series feature set and reproduced performance in (Umeda [2017]) to compare to this baseline. We saw that the performance of this baseline actually outperforms the TDA feature engineered experiment as reported. This suggests that for a task of this type the TDA approach is not SOTA, but may hold value in other regimes, or under more specific hyperparameter tuning. Building on these results, we explored the novel geometric feature engineering method of persistent eigenvalues of the Laplacian. This method also outperforms TDA, but does not outperform the raw time series experiment.

We showed the performance of these networks under the strain of reduced data samples, and in resolution reduction. The impact on performance as we iterate through the parameter space is relatively smaller for the eigenvalue features, but performance remains worse than the raw time-series.

Finally, we provided a test-bed for further iteration on these sorts of prediction tasks, and opened up a discussion around sensor resolution, sample data size, downsampling, feature engineering, and CNNs. The comparison pipelines are easily extensible for further experimentation with this dataset or others. All of the code for feature engineering and testing is available on GitHub.

Variable resolution training has been employed on ImageNet (Howard [2018]) to dramatically reduce training time, it’s interesting to consider the implications of explicitly controlling downsampling

schemes for this ansatz. Larger scope, we have left open the question of “multi-resolution” sensor networks and the impact on geometric feature engineering and downsampling.

References

- Ralph G. Andrzejak, Klaus Lehnertz, Florian Mormann, Christoph Rieke, Peter David, and Christian E. Elger. Indications of nonlinear deterministic and finite-dimensional structures in time series of brain electrical activity: Dependence on recording region and brain state. *Phys. Rev. E*, 64:061907, Nov 2001. doi: 10.1103/PhysRevE.64.061907. <https://link.aps.org/doi/10.1103/PhysRevE.64.061907>.
- M. M. Bronstein, J. Bruna, Y. LeCun, A. Szlam, and P. Vandergheynst. Geometric deep learning: Going beyond euclidean data. *IEEE Signal Processing Magazine*, 34(4):18–42, 2017.
- Frédéric Chazal and Bertrand Michel. An introduction to topological data analysis: fundamental and practical aspects for data scientists. *ArXiv*, abs/1710.04019, 2017.
- Fan RK Chung and Fan Chung Graham. *Spectral graph theory*. American Mathematical Soc., 1997.
- Ian C. Covert, Balu Krishnan, Imad Najm, Jiening Zhan, Matthew Shore, John Hixson, and Ming Jack Po. Temporal graph convolutional networks for automatic seizure detection. In Finale Doshi-Velez, Jim Fackler, Ken Jung, David Kale, Rajesh Ranganath, Byron Wallace, and Jenna Wiens, editors, *Proceedings of the 4th Machine Learning for Healthcare Conference*, volume 106 of *Proceedings of Machine Learning Research*, pages 160–180, Ann Arbor, Michigan, 09–10 Aug 2019. PMLR. URL <http://proceedings.mlr.press/v106/covert19a.html>.
- Meryll Dindin, Yuhei Umeda, and Frederic Chazal. Topological data analysis for arrhythmia detection through modular neural networks. In Cyril Goutte and Xiaodan Zhu, editors, *Advances in Artificial Intelligence*, pages 177–188, Cham, 2020. Springer International Publishing. ISBN 978-3-030-47358-7.
- H. Edelsbrunner, D. Letscher, and A. Zomorodian. Topological persistence and simplification. In *Proceedings of the 41st Annual Symposium on Foundations of Computer Science*, FOCS ’00, page 454. IEEE Computer Society, 2000. ISBN 0769508502.
- Herbert Edelsbrunner, David Letscher, and Afra Zomorodian. Topological persistence and simplification. *Discrete & Computational Geometry*, 28(4):511–533, Nov 2002. ISSN 1432–0444. doi: 10.1007/s00454--002--2885--2.
- W. D. Hall. Representation of blacks, women, and the very elderly (aged > or = 80) in 28 major randomized clinical trials. *Ethnicity and disease*, 9(3):333–340, 1999.
- Allen Hatcher. *Algebraic topology*. Cambridge Univ. Press, Cambridge, 2000. URL <https://cds.cern.ch/record/478079>.
- Jeremy Howard. Now anyone can train imagenet in 18 minutes. <https://www.fast.ai/2018/08/10/fastai-diu-imagenet/>, 2018.
- Prasun Roy, Subhankar Ghosh, Saumik Bhattacharya, and Umapada Pal. Effects of degradations on deep neural network architectures. *CoRR*, abs/1807.10108, 2018. <http://arxiv.org/abs/1807.10108>.
- R. Scopigno, D. Zorin, Gunnar Carlsson, Afra Zomorodian, Anne Collins, and Leonidas Guibas. Persistence barcodes for shapes, 2004.
- Youngjoo Seo, Michaël Defferrard, Pierre Vandergheynst, and Xavier Bresson. Structured sequence modeling with graph convolutional recurrent networks. *arXiv*, 2016. URL <https://arxiv.org/abs/1612.07659>.
- Sveinn Steinarrson. Downsampling time series for visual representation. Master’s thesis, University of Iceland, 2013.
- Yuhei Umeda. Time series classification via topological data analysis. *Transactions of the Japanese Society for Artificial Intelligence*, 32(3):D–G72_–12, 2017. doi: 10.1527/tjsai.D--G72.

Afner JS. Veinot TC, Mitchell H. Good intentions are not enough: how informatics interventions can worsen inequality. *J Am Med Inform Assoc.*, 25(8):1080–1088, 2018.

Z. Wang, W. Yan, and T. Oates. Time series classification from scratch with deep neural networks: A strong baseline. In *2017 International Joint Conference on Neural Networks (IJCNN)*, pages 1578–1585, 2017.

Afra Zomorodian and Gunnar Carlsson. Computing persistent homology. In *Proceedings of the Twentieth Annual Symposium on Computational Geometry*, SCG '04, pages 347–356, New York, NY, USA, 2004. Association for Computing Machinery. ISBN 1581138857. doi: 10.1145/997817.997870.

Acknowledgements

The authors thank the anonymous reviewers from the NeurIPS 2020 TDA And Beyond Workshop.

We extend heartfelt appreciation to Will Chernoff for excellent feedback on the manuscript including a careful review of the possible implications of this work, leading to the broader impacts section.

We also thank Dan Marthaler, Sven Schmit, and Hector Yee for feedback and comments on the manuscript.

Janu Verma provided detailed feedback and recommendations on the exposition.

Broader Impacts

As the primary application of study for these experiments lies within the medical space, both positive and negative applications jump to mind. Large, high-resolution datasets both for training and evaluation come at the benefit of those in developed and wealthy communities. Our research – through its focus on developing methods robust to degradation – provides an opportunity for an improvement in prediction methods in lower fidelity data regimes; i.e. methods designed with downsampling and data reduction in mind alleviate needs for larger and more complete datasets.

The present study examines EEGs and eye states, which could easily extend to other ailments. More accurate models for predicting seizure, for example, could greatly benefit those privileged enough to share characteristics with those used to train the model in the first place. But what of those not sampled?

As (Hall [1999]) has observed: Blacks, women, and the elderly have historically been excluded from clinical trial research. Such arrangements can lead to what (Veinot TC [2018]) has referred to as intervention-generated inequalities (IGI), a social arrangement where one group gets better, while others don't. On top of their original ailments, groups left out are burdened with continued medical involvement and the associated costs (e.g. additional tests, transportation, childcare, and missed opportunities).

We offer the following suggestions for those in the medical industry hoping to combat some of this inequity: 1. Insist on multiple representative datasets including those from underrepresented groups – incentivization where appropriate. 2. Identify and assist in eliminating barriers to involvement in data collection or diagnostics.

A Appendix: Persistent Homology

Fix $\epsilon \geq 0$, and let $X = \{x_1, \dots, x_n\}$ be an enumerated subset of \mathbb{R}^m . For $k = 0, 1, \dots$ define $C_{\epsilon, k}$ to be the \mathbb{R} -vector space whose formal basis is given by all subsets of X of the form

$$\{(x_{i_0}, x_{i_1}, \dots, x_{i_k}) \text{ such that } i_0 < i_1 < \dots < i_k \text{ and } \|x_{i_\alpha} - x_{i_\beta}\| < \epsilon \text{ for all } \alpha, \beta = 0, 1, \dots, k\}.$$

We take $C_{\epsilon, k}$ to be the zero vector space if there are no such subsets. There are linear maps $\partial_k : C_{\epsilon, k} \rightarrow C_{\epsilon, k-1}$ defined by

$$\partial_{\epsilon,k}(x_{i_0}, \dots, x_{i_k}) = \sum_{j=0}^k (-1)^j (x_{i_0}, \dots, \widehat{x_{i_j}}, \dots, x_{i_k})$$

where $(x_{i_0}, \dots, \widehat{x_{i_j}}, \dots, x_{i_k})$ denotes the element $(x_{i_0}, \dots, x_{i_{j-1}}, x_{i_{j+1}}, \dots, x_{i_k}) \in C_{\epsilon,k-1}$. One can check that $\text{Im}(\partial_{\epsilon,k+1}) \subseteq \text{Ker}(\partial_{\epsilon,k})$. The k^{th} ϵ -homology group of X is defined to be the vector space quotient $H_{\epsilon,k}(X) := \text{Ker}(\partial_{\epsilon,k}) / \text{Im}(\partial_{\epsilon,k+1})$. The k^{th} ϵ -Betti number of X is defined to be $\beta_{\epsilon,k}(X) := \dim(H_{\epsilon,k}(X))$. Intuitively, $\beta_{\epsilon,k}(X)$ measures the number of k -dimensional holes in the point cloud X at resolution ϵ . We will typically write $\beta_k(\epsilon)$, and allow ϵ to vary over a fixed range $[0, r]$. We will also refer to $\beta_k(\epsilon)$ as an ϵ -series. In the sequel, *persistent homology* will in general refer to the collection of β_k 's, as they capture information about how the homology persists over varying resolutions. (c.f. Hatcher [2000])

B Appendix: Downsampling

B.1 Time series downsampling

We consider a downsampling a selection of a subsequence of points, or a smaller set of points that summarize the timeseries. We assume the timeseries has $n + 2$ points, and construct a downsample of $m + 2$ points.

Naive Bucketing: Select the first and last points of the timeseries; cover the the rest of the points with m even-width intervals(up to integer rounding). We call this a *bucketing*.

Consider a sequence of sequences:

$$\{\{x_0\}, \{x_1, \dots, x_k\}, \{x_{k+1}, \dots, x_{2k}\}, \dots, \{x_{(m-1)k+1}, \dots, x_{mk}\}, \{x_{n+1}\}\}$$

and for simplicity, call the sub-sequences $\{b_i\}_{0 \leq i \leq n+1}$ such that $b_0 = \{x_0\}$, $b_{n+1} = \{x_{n+1}\}$, and $b_j = \{x_{(j-1)k+1} \dots x_{(j-1)k}\}$, we refer to these as *buckets*.

Dropout: For each bucket, select the first point in the subsequence.

Bucket Averaging: For each bucket in a naive bucketing, average the x and y coordinates and take this as the representative point; take also the first and last points.

For a bucket, we compute the 2-dimensional average of the points contained within: μ_j . For convenience of notation, we write elements of b_i , as $\{x_i^j\}$.

Largest-Triangle Three-Bucket Downsample (LTTB) We compute the subsequence via the optimization problem:

$$\text{compute } l_i = \arg \max_{x_i^j} \Delta \left(l_{i-1}, x_i^j, \mu_{i+1} \right) \text{ such that } l_0 = b_0 \text{ and } \mu_{n+1} = b_{n+1}.$$

The sequence $\{l_0, \dots, l_{n+1}\}$ is the *largest triangle three bucket downsample*. For more details and intuition around this construction we recommend the original paper.

Remark 1. *This is computed via a recursive optimization process iterating through the buckets; a non-recursive formulation to find the global optima is also possible. The distinction between these two solutions is that in the recursive solution each optimization is conditioned on the previous bucket, where-as the global solution conditions on all buckets simultaneously.*

B.2 Dynamic downsampling

In the above bucketing strategies, points in all regions of the time series are given equal weight in the downsample. Often times, the lagging-variance of a time series is not uniform across the time-domain. One might expect that regions of higher variance might warrant higher resolutions in the downsample, while low variance might require lower resolutions. A simple implementation of this idea, (*inspired by Steinarsson [2013]*) is demonstrated in Algorithm 1(implementation included in Appendix). Downsampling methods are then applied to this bucketing of the timeseries.

Algorithm 1 Variance weighted dynamic bucketing

Precondition: \mathcal{B} a naive bucketing, and P an iteration count

```
1: function DYNAMICBUCKETS( $B : \text{List}[\text{List}[\text{Float}]]$ )
2:    $[b_j] \leftarrow \mathcal{B}$ 
3:   for  $i \leftarrow 1$  to  $P$  do
4:     for  $j \leftarrow 1$  to  $m$  do
5:        $S(b_j) \leftarrow \text{SSE}(\text{OLS}(b_j))$ 
6:        $z \leftarrow \arg \max_j (S(b_j))$ 
7:        $b_z^l \leftarrow \{x_1^z, \dots, x_{\lfloor k/2 \rfloor}^z\}$ 
8:        $b_z^r \leftarrow \{x_{\lfloor k/2 \rfloor + 1}^z, \dots, x_k^z\}$ 
9:        $\mathcal{B} \leftarrow \mathcal{B} \setminus \{b_z\} \cup \{b_z^l, b_z^r\}$ 
10:    for  $i \leftarrow 1$  to  $P$  do
11:      for  $j \leftarrow 1$  to  $m + P$  do
12:         $S(b_j) \leftarrow \text{SSE}(\text{OLS}(b_j))$ 
13:         $a \leftarrow \arg \min_a (S(b_a) + S(b_{a+1}))$ 
14:         $b_a^* \leftarrow \{x_1^a, \dots, x_k^a\} \cup \{x_1^{a+1}, \dots, x_k^{a+1}\}$ 
15:         $\mathcal{B} \leftarrow \mathcal{B} \setminus \{b_a, b_{a+1}\} \cup \{b_a^*\}$ 
16:    return  $\mathcal{B}$ 
```

Remark 2. Rather than serially splitting, and then combining buckets to arrive at the rebucketing, it's natural to ask how alternating these operations effects the result. The authors carried out several simulations of this technique and found that convergence to 'stable' bucketing took place much more quickly, but produced far worse results with respect to total SSE.

B.3 Dynamic downsampling results

We tested our dynamic downsampling strategies for the Laplacian eigenvalues features.

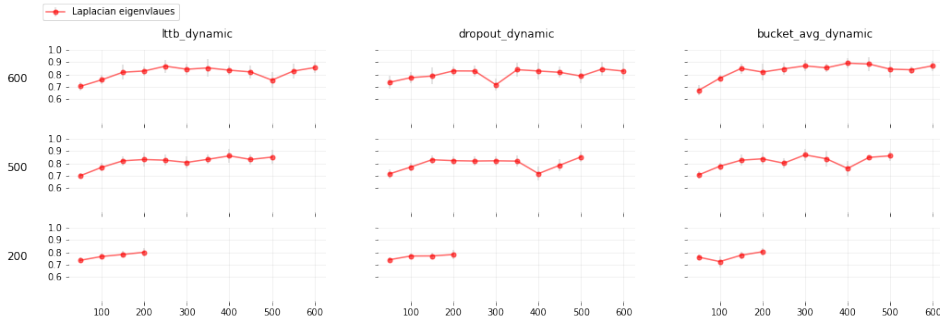


Figure 5: Experiment results for dynamic bucketing downsampling methods. Diagram columns refer to downsampling method. Diagram rows correspond to initial length of time-series segment, with each point reflecting number of points after downsampling. Within rows, y-axis is accuracy on binary cross-entropy, x-axis is the number of points in the time-series samples.

C Appendix: Cartoon version of this paper

We thought it would be fun to capture the methods of this paper in a cartoon. The following image has a few numbered paths to walk through the three feature generation paths.

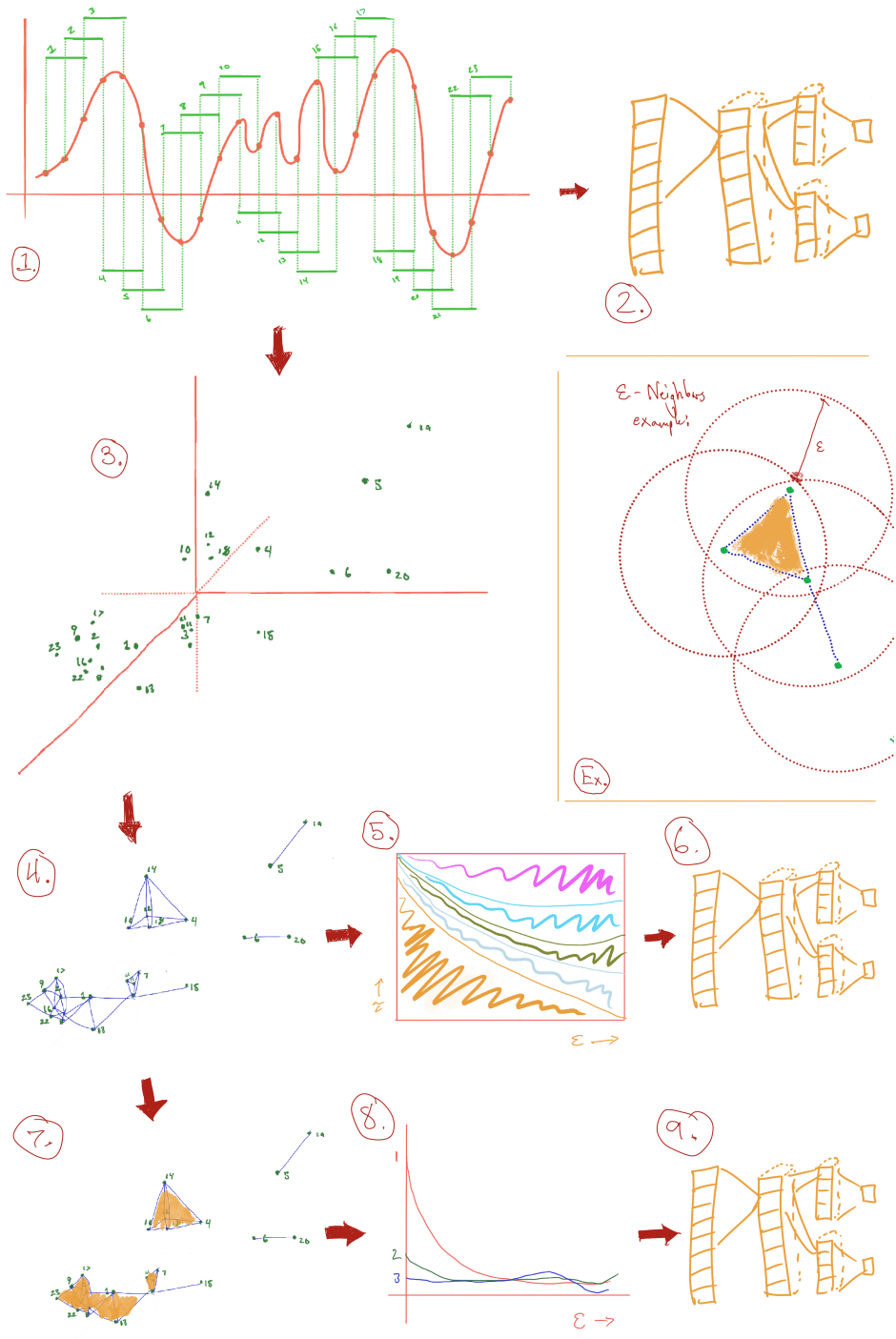


Figure 6: Three model pipelines. (1 → 2) Direct CNN on the raw features. (1 → 3) Takens' embedding. (3 → 4) generating the neighbor graph. (4 → 5) persistent Spectrum. (4 → 7) persistent Betti numbers. (5 → 6, 8 → 9) CNN's from geometric features. (Ex.) ϵ -neighbors for four points in turquoise.